frontiers in Earth Science

ORIGINAL RESEARCH
published: 30 July 2021
doi: 10.3389/feart.2021.678655

Studies for Frost Heave Characteristics and the Prevention of the High-Speed Railway Roadbed in the Zoige Wetland, China

Fujun Niu[1,2,3], *He Hu*[1,2]*, *Minghao Liu*[3]*, *Qinguo Ma*[1,2] *and Wenji Su*[1,2]

[1]State Key Laboratory of Subtropical Building Science, South China University of Technology, Guangzhou, China, [2]South China Institution of Geotechnical Engineering, School of Civil Engineering and Transportation, South China University of Technology, Guangzhou, China, [3]State Key Laboratory of Frozen Soil Engineering, Northwest Institute of Eco-Environment and Resources, Chinese Academy of Sciences, Lanzhou, China

OPEN ACCESS

Edited by:
Guo Donglin,
Institute of Atmospheric Physics (CAS), China

Reviewed by:
Yanhu Mu,
Chinese Academy of Sciences (CAS), China
Alan Rempel,
University of Oregon, United States
Qingbai Wu,
Chinese Academy of Sciences (CAS), China

***Correspondence:**
He Hu
1204071132@qq.com
Minghao Liu
liuminghao@lzb.ac.cn

Specialty section:
This article was submitted to Cryospheric Sciences, a section of the journal Frontiers in Earth Science

Received: 10 March 2021
Accepted: 28 June 2021
Published: 30 July 2021

Citation:
Niu F, Hu H, Liu M, Ma Q and Su W (2021) Studies for Frost Heave Characteristics and the Prevention of the High-Speed Railway Roadbed in the Zoige Wetland, China. Front. Earth Sci. 9:678655. doi: 10.3389/feart.2021.678655

The Xining–Chengdu high-speed railway crosses the Zoige Wetland, located on the northeast edge of the Qinghai-Tibet Plateau and the upper reaches of the Yellow River. The cold climate and frost-heave-sensitive subgrade soil cause a large frost heave deformation of the roadbed, threatening the safety of trains. This article systematically studied the ground temperature development, frost heave characteristics, soil water content, and groundwater level variations by field investigation and monitoring. The maximum frost heave deformations of the natural flat ground and hillslope reached 25.64 and 3.17 mm, respectively, and this significant discrepancy was mainly caused by the groundwater supply conditions. Future roadbed stability on the flat ground may be compromised by frost heave deformation. To solve this problem, contrasting indoor tests were conducted to analyze the frost heave characteristics of natural ground clay and replacement coarse-grained soil (CGS). It was shown that the absorbed external water mainly changed into dispersed pore ice in the freezing CGS, while it mainly changed into the layered ice lens in the freezing clay. Further tests showed that the frost susceptibility of the CGS was proportional to the fines content and initial water content. The poorly graded CGS had weaker frost susceptibility than the well-graded CGS. The results suggest that anti-frost methods should be fully considered, including strict control of fines content and water content, prioritizing the use of poorly graded filling, and disruption of local water accumulation in the filling layer.

Keywords: zoige wetland, high-speed railway, frost heave prevention, coarse-grained soil, field monitoring

INTRODUCTION

High-speed railways (HSRs) have been constructed to improve traffic congestion and develop local economies in China in recent years. It has been reported that the total length of HSR in China will reach 38,000 km by 2025. In northwest China, particularly in and around the Qinghai–Tibet Plateau, undeveloped transportation infrastructure seriously restricts local economic development. Therefore, HSR construction is essential and necessary. Long-distance railway and complex geo-engineering conditions make HSR construction extremely difficult. Among the difficulties, thaw settlement in permafrost regions and frost heave in the seasonally frozen ground should be paid

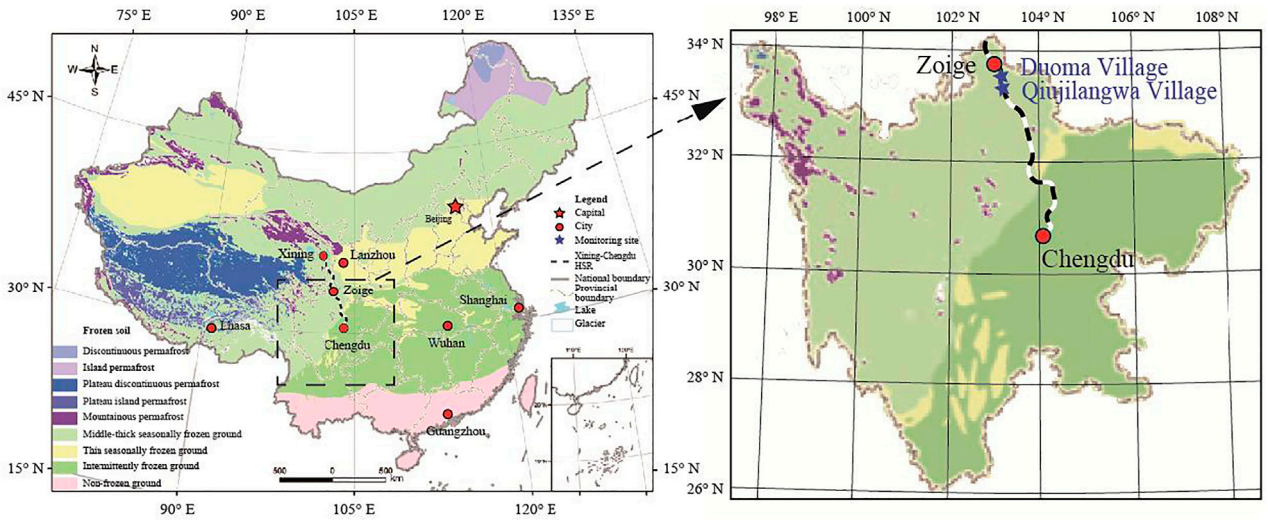

FIGURE 1 | Frozen ground distribution in China and the monitoring site along the Xining-Chengdu HSR.

particular attention to because these regions largely consist of permafrost and seasonally frozen soils (Jin, 2007; Yue et al., 2007; Li et al., 2008; Song et al., 2014; Wang et al., 2020). The cold climate and frost heaving of the subgrade significantly affect the safety and stability of railway lines. A new high-speed railway between Xining (Capital of the Qinghai Province) and Chengdu (Capital of the Sichuan Province) began construction in 2020 and is planned to be completed in 2027. The whole line passes through vast areas of seasonally frozen ground, especially the Zoige section of the swamp wetland located in the northeast part of the Qinghai–Tibet Plateau and the upper reaches of the Yellow River (**Figure 1**). Wet soils, shallow groundwater, and lower temperatures in this area seriously threaten railway stability through frost heaving.

Frost heaving was first investigated by Taber (1929) and has been widely studied using indoor freezing tests and numerical analyses (Everett, 1961; Gilpin, 1980; Konrad, 2008; Thomas et al., 2009; Jin et al., 2019; Xu et al., 2020). Many models have been developed to predict frost heave deformation, including the hydrodynamic model (Harlan, 1973), the rigid-ice model (O'Neill and Miller 1985), the segregation potential model (Konrad and Morgenstern, 1981), and the discrete ice lens model (Nixon, 1991). It is widely agreed that ice lenses caused by water transportation dominate soil deformation. Therefore, eliminating ice lenses is the most effective measure for preventing frost heaving. The formation of ice lenses is closely related to soil type, water content and water migration conditions, temperature and temperature differences, freezing rate, and load (Taber, 1929; Miller, 1972; Gilpin, 1980; Konrad and Morgenstern, 1982; Peppin and Style, 2012; Mao et al., 2014).

The common HSR embankment filling is coarse-grained soil (CGS), which consists of coarse grains and a certain content of fine grain soil. The particle size of the fine grain is less than 0.075 mm. For the freezing CGS, the low unfrozen water content and large void volume make it difficult for ice lenses to form. However, based on field observations along the Harbin–Dalian HSR (HDHR) and Lanzhou–Xinjiang HSR, frost heave still occurred (Liu et al., 2016; Lin et al., 2018). Niu et al. (2017) reported the measured soil water, ground temperatures, and deformation variations of embankments and cut sections in the HDHR. The frost heave deformation discrepancy between two different types of subgrade indicated that soil water content was the primary factor controlling the frost heave amount, while frost depth was the secondary factor. Zhang et al. (2016) and Sheng et al. (2014) proposed the three most likely frost heave mechanisms in the HSR foundation: the high fine content caused by poor quality control of the coarse filling, the top-down water supply mechanism resulting from the flow of rainfall water and other surface water, and the bottom-up water supply mechanism caused by mud pumping under train cyclic loads. A corresponding one-dimensional frost heave model was developed to verify these mechanisms (Sheng et al., 1995; Sheng et al., 2013). It was concluded that the three mechanisms interacted with each other, and their synergetic action caused the observed frost heave deformation of the HSR embankment. Wang et al. (2016) demonstrated that moisture content was the most significant contributing factor to the frost heave ratio of the CGS. If the moisture content was maintained at less than 5%, the frost heave development of the CGS could be prevented. Based on these studies, it is widely agreed that the fines content, water content, and filling type have significant influences on the frost susceptibility of the CGS. However, previous studies mainly focused on the relationships between frost heave deformation and content of the fine grain and ignored the important role of grain size distribution in CGS. Therefore, the impact of soil gradation should be investigated further.

The purpose of this research was to study the frost heave characteristics of HSR roadbeds in the Zoige Wetland and corresponding prevention. To achieve this, a comprehensive

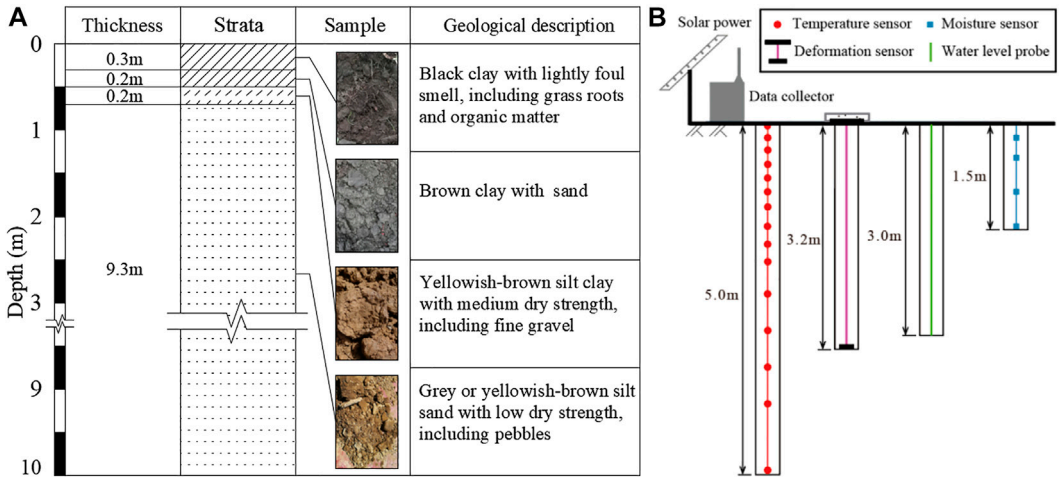

FIGURE 2 | Geotechnical condition and field-monitoring system at the study sites. **(A)** Geotechnical condition; **(B)** schematic diagram of monitoring system.

field-monitoring system was installed to monitor the variations in ground temperature, ground deformation, soil moisture, and groundwater table. Based on the monitoring data and local ecological environment, a soil-replacement method with CGS was proposed to reduce the frost heave deformation of the embankment. Then, the effectiveness of this method was tested in terms of the frost heave amount and frost heave ratio using indoor experiments. Moreover, further experiments were performed to study the influences of various typical factors on the anti-frost effect of the replacement method, including the fine content, initial water content, and grain size distribution of coarse particles. Finally, the frost heave characteristics of filling were studied to provide potential engineering treatments for HSR embankments in cold regions. The results can provide useful guidance for frost heave prevention in road construction in seasonally frozen ground.

FIELD MONITORING OF NATURAL GROUND

Study Site Condition

The construction of the Xining–Chengdu HSR began in March 2020, and the planned construction period was 7.5 years. To observe the frost heave characteristics of the soils underlying the railway line, two monitoring systems were installed at Qiujilangwa village and Duoma village, near the city of Zoige, Sichuan Province (**Figure 1**). The Qiujilangwa village monitoring site is located on flat ground approximately 48 km southeast of Zoige city. The Duoma village monitoring site is located on a hillslope approximately 11 km southeast of Zoige city. Field investigations showed that the natural shallow strata of these two monitoring sites were the same. The strata are composed of black clay with grass roots and organic matter at a depth of 0–0.3 m, brown clay with sand at a depth of 0.3–0.5 m, yellowish-brown silt clay with fine gravel at a depth of 0.5–0.7 m, and yellowish-brown silt sand with pebbles at depths below 0.7 m. The corresponding field photos of the samples are shown in **Figure 2A**.

Monitoring System

Field monitoring was performed under a natural surface. The monitoring system consisted of an automatic data collector, a power supply system, temperature sensors, moisture sensors, deformation sensors, and a water level probe (**Figure 2B**). The variations in soil temperature, moisture content, groundwater table, and deformation caused by freezing and thawing were collected. The temperature sensors were designed and produced by the State Key Laboratory of Frozen Soil Engineering, and the normal measurement range of the sensor was −25 to +80°C. In total, 16 temperature sensors with an accuracy of ±0.02°C were installed in a 5 m-deep borehole with a thermistor string (Wu et al., 2018; Miao et al., 2020). The spacing of the temperature sensors was 0.2 m in the top, 1.0 m, 0.25 m from 1.0 to 2.0 m in depth, and 0.5 m from 2.0 to 5.0 m in depth.

The volumetric water content of the soil was measured using four QSY8909A soil-moisture sensors (Sichuan Stone Edge Science and Technology Co., Ltd.) at depths of 0.2, 0.5, 1.0, and 1.5 m. The moisture sensors had a measurement range of 0–100% and an accuracy of 3% (Lin et al., 2018). In addition, a QSY8907C-200 frost heave sensor (produced by Sichuan Stone Edge Science and Technology Co., Ltd) was used to measure the frost heave amount. The maximum frost depth of natural ground is less than 1.0 m (The National Standards Compilation Group of the People's Republic of China, 2011). The soil layers deeper than 3.2 m are far from the frost front, and the corresponding deformation can be negligible. Thus, a depth of 3.2 m can be taken as a benchmark. The frost heaving sensor was embedded into the soil through a plastic pipe. This sensor measured the relative deformations between the top and bottom plates, as shown in **Figure 2B**. The bottom plate was fixed to a designated depth of 3.2 m by concrete, and the top plate was fixed to the natural ground surface. During the freezing season, the top plate moves up as frost heave occurs. The frost heave

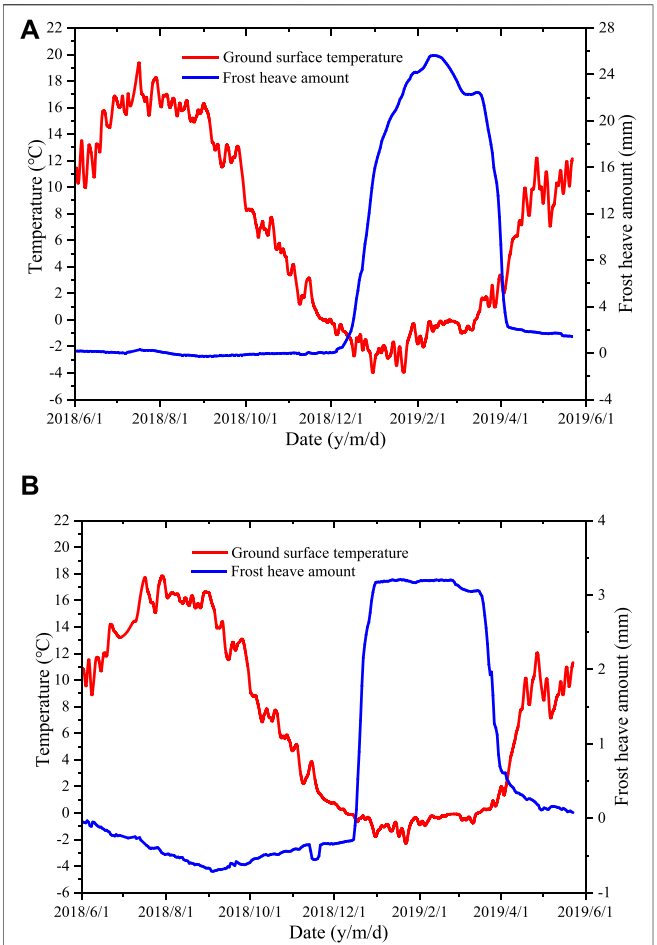

FIGURE 3 | Variations of the ground surface temperature and frost heave amount. **(A)** Data from the Qiujilangwa village monitoring site; **(B)** data from the Duoma village monitoring site.

amount of natural ground can be determined by measuring the displacement of the top plate. The measurement accuracy and measurement range of the heave sensor are 0.01 mm and from −100 mm to +100 mm, respectively. Finally, a HOBO U20-001-01 water level probe was installed in a 3.0 m-deep borehole to record the groundwater table variation automatically. All sensors were connected to a QSY300Z-64CH automatic data collector. The monitored data were automatically collected and transmitted wirelessly. All instruments in this monitoring system were powered by a combination of solar panels and storage batteries. Monitoring data were recorded every 4h from June 2018 through May 2019.

Soil Temperature and Frost Heave Amount

The Qiujilangwa village monitoring site is located on flat ground. According to the monitored data, the ground surface temperature reached a maximum value of 19.4°C in late July 2018 and a lowest value of −4.1°C in late January 2019, as shown in **Figure 3A**. The annual range of surface temperature and mean annual surface temperature were 23.5 and 6.6°C, respectively. The surface temperature dropped to less than 0°C on November 26 and continued until March 13. The freezing period of the ground was approximately 107 days. At this time, the rapid frost heave developed and reached a maximum value of 25.64 mm on February 13, 2019. Following this period of rapid heave, the displacement decreased from February 13 to March 13 to a stable value of 22.44 mm accompanied by the approach of 0°C isotherm. As the temperature further increased and the soil continued thawing, the displacement rapidly decreased to 2.28 mm within 20 days. The final deformation amount was approximately 1.66 mm during the next thaw period. The melting amount was less than the frost heave amount after the freeze–thaw action. We infer that this was because the soil resisted the thaw settlement because of its cohesion. If the number of freeze–thaw cycles increases, the soil cohesion strength will decrease due to water migration. Eventually, the thaw settlement amount would be close to the frost heave amount.

The frost heave ratio is defined as the proportion that the heave amount accounts for frozen depth:

$$\eta = \frac{\Delta h}{H_f} \times 100\% \quad (1)$$

where η is the frost heave ratio, Δh is the frost heave amount (mm), and H_f is the frozen depth (mm).

The contour graphs of the subsurface temperature show temperature distribution using the time as the X-axis, the stratum depth as the *Y*-axis (**Figure 4**). The unmeasured temperatures were obtained based on the least-squares method according to the measured temperatures. According to the current code for engineering geological investigation of frozen ground in China (The National Standards Compilation Group of the People's Republic of China, 2014), the grades of the frost-susceptible silt clay can be classified as grade Ⅰ non-frost soil with a frost heave ratio less than 1%, grade Ⅱ weakly frost-susceptible soil with a frost heave ratio larger than 1% and less than 3.5%, grade Ⅲ frost-susceptible soil with a frost heave ratio larger than 3.5% and less than 6%, grade Ⅳ highly frost-susceptible soil with a frost heave ratio larger than 6% and less than 12%, and grade Ⅴ extra highly frost-susceptible soil with a frost heave ratio larger than 12%. The frozen depth of the Qiujilangwa village monitoring site was 0.42 m when the frost heave amount reached the maximum, based on the contour graph of subsurface temperature shown in **Figure 4A**. At that moment, the frost heave ratio was 6.10%, indicating that the ground soil could be regarded as a grade Ⅳ highly frost-susceptible soil. In addition, the maximum frozen depth (0.54 m) occurred on January 23, 2019, but the heave amount increased until February 23, 2019. This indicates that the frost heave amount was hysteretic to the frost penetration. Owing to the relatively shallow frost penetration and the rapidly rising ground surface temperature after March 13, the frozen depth dropped to zero within four days.

The Duoma village monitoring site is located on a gentle hillslope. The ground surface temperature also began to drop to subzero temperatures on December 10 (**Figure 3B**). Rapid

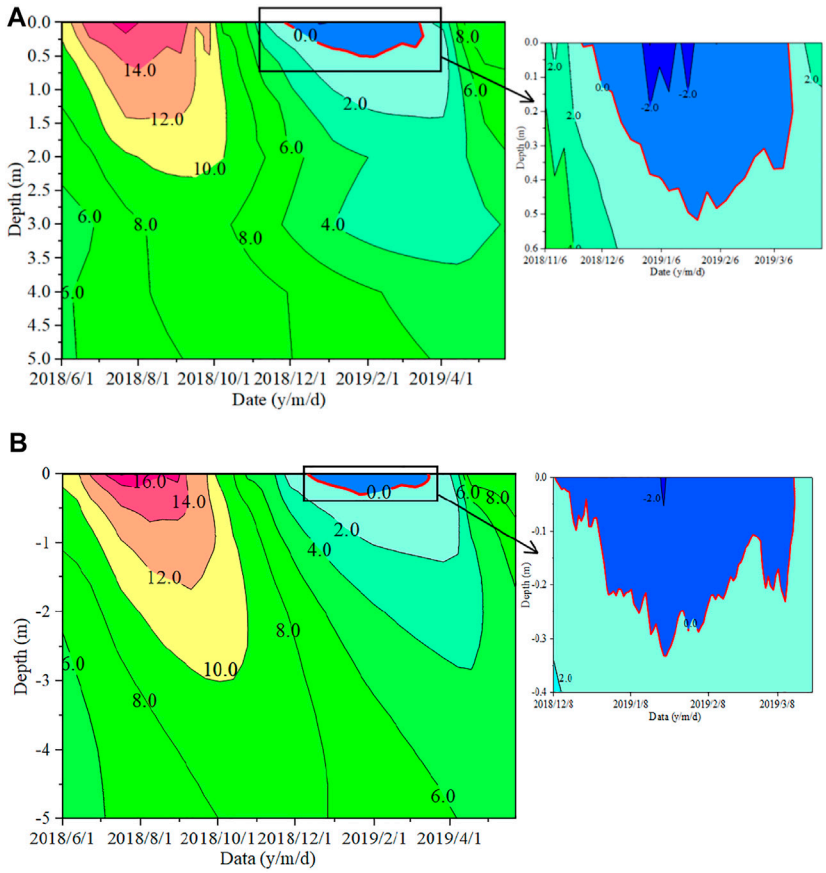

FIGURE 4 | Contour graph of subsurface temperature. **(A)** Data from the Qiujilangwa village monitoring site; **(B)** data from the Duoma village monitoring site.

heaving was recorded immediately accompanied by soil freezing. However, the frost heave amount did not show a successive increasing tendency, but it rapidly reached a maximum value of 3.17 mm on December 31 and then remained stable until the beginning of the thawing season on March 16. The frozen depth on December 31 was 0.22 m, and the corresponding frost heave ratio was 1.45% (**Figure 4B**). The ground soil could be regarded as grade II, weakly frost-susceptible soil. The maximum frozen depth (0.33 m) also occurred on January 23, 2019. Furthermore, most thawing settlement occurred over 27 days (March 16 to April 12), reaching 0.34 mm. The highest and lowest ground surface temperatures at the Duoma village monitoring site were 18.5°C and −3.6°C, respectively, similar to the values at the Qiujilangwa village monitoring site (19.4°C and −4.1°C). However, the frost heave displacement at the Duoma village monitoring site was much less than that at the Qiujilangwa village monitoring site.

Soil Moisture Content

The soil moisture content changes with time at different depths for the Qiujilangwa village monitoring site are shown in **Figure 5A**. From July to early September, the moisture content at a depth of 0.2 m gradually decreased to 28.0%, which was attributed to evaporation. This is because the variation of soil moisture content at the shallow surface is related to evaporation, precipitation, vegetation conditions, temperature, and human activity. The Qiujilangwa village monitoring site did not experience any special or large variations of vegetation conditions and human activity from July 2018 to early September 2018. At the same time, the precipitation was small. The subsurface temperature between July and early September was large (**Figure 4**), which was beneficial to water evaporation. Following this process, the water content rapidly increased from September 3 to September 26 to a nearly stable level of approximately 39.2% because of the decrease in subsurface temperature and increase in rainfall. When the surface temperature fell below 0°C, the water content did not rapidly decrease to 9.8% until December 18. This could be because of the phase change of the liquid water into ice. The soil-water sensor only measured the unfrozen liquid water content. In the following frozen period, the unfrozen water content at a 0.2 m depth maintained a stable value of 8%. After March 13, the soil moisture content increased rapidly as the surface temperature increased, and the soils melted during the thawing season.

In the Qiujilangwa village monitoring site, the moisture content variation at a 0.5 m depth was similar to that at a

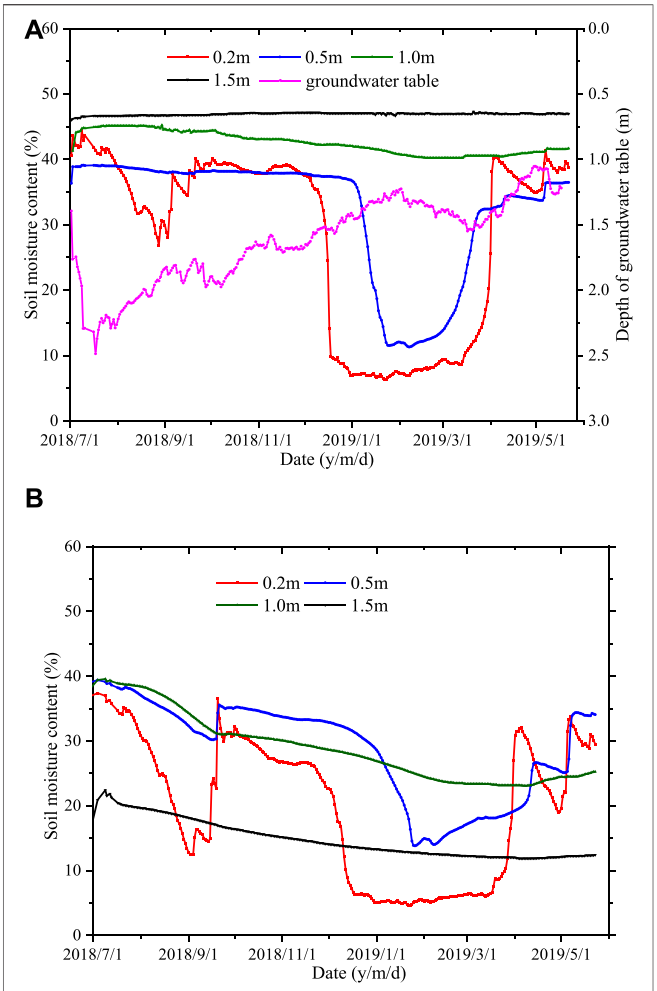

FIGURE 5 | Depth of groundwater table and soil moisture content at various depths. **(A)** Data from the Qiujilangwa village monitoring site; **(B)** data from the Duoma village monitoring site.

0.2 m depth in winter. However, it showed a rapid falling trend on January 6 and a slow rising tendency on February 24, indicating that the corresponding freezing period was less than that at a 0.2 m depth. The steady unfrozen water content during the freezing season was approximately 11.5%. The near-surface soil water content fluctuated acutely with freezing and thawing. Furthermore, the 1.0-m-deep position was far from the frozen depth, but it still showed a slow changing trend in water content from December 2018 to March 2019. The water content changes were caused by moisture migration to the frozen zone and melted ice from the upper-layer frozen soil, respectively. As a result of the approach of the groundwater table (**Figure 5A**), the water content at the 1.5 m depth maintained a steady value of 47.0% during the entire monitoring period. The groundwater table showed a sharply decreasing trend in the initial monitoring time and a slowly growing tendency during the following phase. The groundwater table also varied around a depth of 1.5 m during the freezing season.

The soil water in the Duoma village monitoring site followed nearly the same pattern as that in the Qiujilangwa village monitoring site, as shown in **Figure 5B**. The data of groundwater table variation at the Duoma village monitoring site were not acquired because of the deep groundwater, indicating that the groundwater table was below a depth of 3 m. The maximum frost depth of the Duoma village monitoring site was approximately 0.54 m. The groundwater was far from the upper frozen soil during the freezing season. In other words, no external water was supplied to the near-surface freezing soil during the freezing season. The soil mainly froze in the pattern of *in-situ* frost heave. As a result, the frost heave displacement at the Duoma village monitoring site was much less than that at the Qiujilangwa village monitoring site and showed a stable value during the freezing season. Thus, the underground water supply condition was the primary limiting factor for frost heaving in the Zoige Wetland.

Based on the aforementioned measurement data, it is thought that the Qiujilangwa village had a shallow frost depth but a large frost heave ratio. The Duoma village had a lower frost heave ratio because of the deep groundwater. Therefore, for running safety, corresponding measures must be taken to prevent the frost heave of HSR embankments in sections similar to the Qiujilangwa village site. Groundwater, negative temperature, and frost-susceptible soil are essential conditions for frost heave development. Frost heave can be mitigated or prevented by controlling any one of the three factors. The Zoige Wetland was identified as a National Nature Reserve in 1998 (Zuo et al., 2019). To protect the local ecological environment and underground water source, the method of lowering or cutting off groundwater to prevent frost heave is not allowed. If the insulation board is installed in the embankment foundation, the possible damage under a long-term train dynamic load is difficult to access. The method of replacing natural soil with CGS seems to be the most reliable choice. Therefore, an appropriate indoor test was designed and conducted to distinguish the frost heave ability of natural foundation soil and CSG.

FROST HEAVE ABILITY OF FOUNDATION SOIL AND COARSE-GRAINED SOIL

Test Description

Materials and Experimental Scheme

Natural soil was taken from the Zoige Wetland, and the plastic limit, liquid limit, optimum water content, and maximum dry density were 16.1, 32.5, 17.2%, and 1.98 g/cm^3, respectively. After drying, crushing, and filtering through a 0.075 mm sieve, the clay sample was prepared with an initial water content of 25.0% and a dry density of 1.58 g/cm^3. The density of the fine clay particles was 2.74 g/cm^3. The CGS samples consisted of a certain amount of the above sieved fine clay and coarse particles (>0.075 mm in size). The density of the coarse particles was 2.55 g/cm^3. The soil sample was placed in a cylindrical sample cell. The soil sample was 10 cm in height and 6 cm in diameter, and the corresponding total volume was approximately 282.73 cm^3. The volume of fine

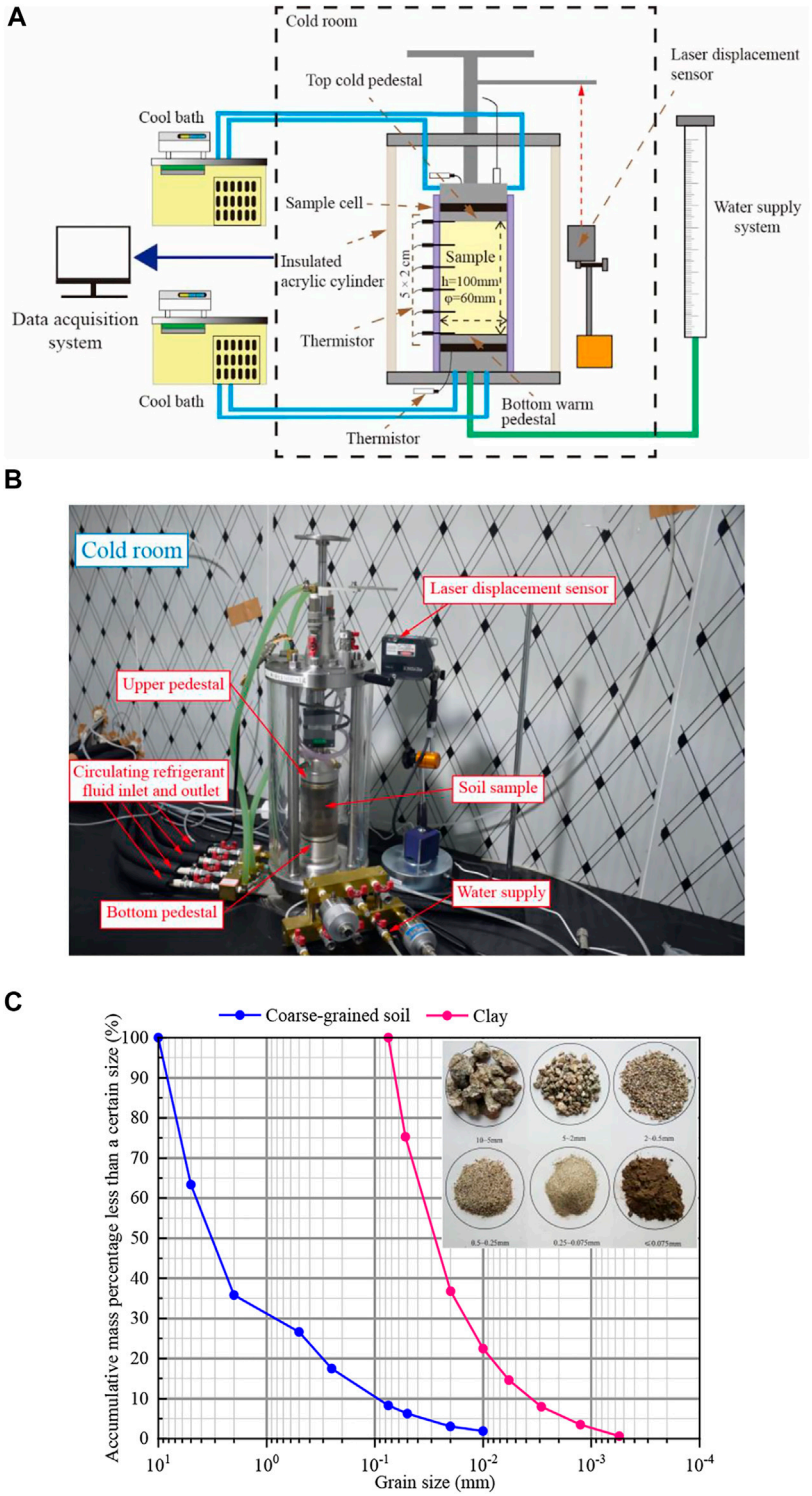

FIGURE 6 | | Frost heave test apparatus and samples. **(A)** Schematic diagram; **(B)** real test devices in the cold room; and **(C)** grain size distribution curves of samples.

clay can be known by dividing its mass by its density. The fines content presented the volume of fine clay as a percentage of the total volume of the sample. The initial water content and fines content of the CGS were 10 and 5.9%, respectively. The dry density of the CGS was 1.95 g/cm^3. The grain size distributions of the CSG and clay are shown in **Figure 6C**.

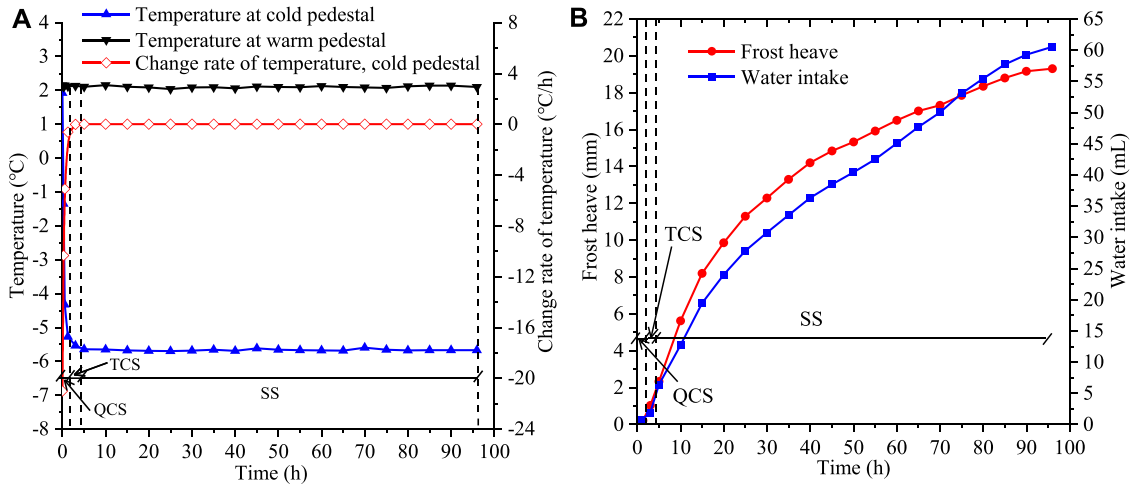

FIGURE 7 | Freezing results of clay sample. **(A)** Variations of temperature and change rate of temperature; **(B)** variations of water intake amount and heave amount.

Test Apparatus and Process

The frost heave test apparatus was composed of six parts: a sample cell, top, and bottom pedestals, two thermal control cool baths, a water supply, a frost heave measuring device, and a data acquisition system (**Figure 6**). The test sample cell was made of organic glass 6 cm in inner diameter, 18.5 cm in height, and 0.75 cm in thickness, and it was used to place the soil sample. Each soil sample was divided into five equal parts, and each part was compacted into a sample cell with a hammer to the target height with a predesigned dry density. At the same time, six Pt 100 thermistors with 2 cm intervals along the sample height were inserted into the soil sample to record the temperature variation at different depths. The sample cell was placed between the fixed bottom pedestal and the vertically movable top pedestal. Two cool baths were connected to the top and bottom pedestals to control the soil temperature. Furthermore, a larger-diameter insulated acrylic cylinder was placed outside the sample cell to reduce heat turbulence from the ambient environment. A Mariotte flask was connected to the bottom pedestal by a plastic tube, and the water level of the Mariotte flask was set at the same height as the bottom of the soil sample to achieve a no-pressure water supply. The frost heave amount was monitored using a laser displacement sensor. The frost heave instruments were placed in a cold room where the room temperature was held at 1°C to maintain the thermal stability of the sample. The data acquisition system consisted of a data logger located outside the cold room and a personal computer. Displacement and temperature data were automatically collected every 5 min.

First, the top and bottom temperatures of the soil sample were kept at +2°C for 12 h to ensure that the initial temperature of the soil sample was uniform. Then, the top and bottom temperatures of the soil sample were set as constant at −6°C and +2°C, respectively, during the entire freezing process. The Mariotte flask was opened simultaneously to provide a moisture source. The frost heave process lasted 96 h for clay and 144 h for CSG. Because of early test carelessness, the soil temperatures in the freezing clay were not measured, but the top cold pedestal and the bottom pedestal were recorded. Because the aim was to determine the frost heave ability of the frozen clay, the unmeasured soil temperature had no effect on this target.

Test Results and Analysis

Frost Heave Characteristics of Natural Clay

The variations in temperature, frost heave, and water intake of clay soil during the freezing process are shown in **Figure 7**. The temperature at the cold pedestal experienced a rapid decrease in the initial freezing stage, followed by a gradual decrease, and an eventual stable state after a period of time (**Figure 7A**). The cooling process was divided into three stages: the quick cooling stage (QCS), transition cooling stage (TCS), and stable stage (SS). The change rate of temperature at the cold pedestal decreased quickly to nearly zero from the QCS to SS, where a negative sign indicated the decrease of temperature. In the QCS and TCS, the frozen depth increased with the downward moving frost front. The amount of liquid water migration was less (**Figure 7B**), and no ice lens was formed because of the short duration. The frost heave amount in these two stages could be regarded as the *in-situ* frost heave amount. The heave with a high frost heave rate was mainly caused by the internal pore water phase changing into ice. The steady stage started when the temperature decreased to the lowest value, and the temperature remained in a stable state after that moment. The frost front almost remained at a fixed height during this stage. Meanwhile, liquid water migration to the frozen zone caused the formation of segregated ice. The frost heave amount at this stage was regarded as the segregated frost heave amount. The final frost heave and water supply amounts were 19.3 mm and 60.5 ml, respectively.

As the water-ice phase in the frozen zone, negative pore water pressure formed, which resulted in successive liquid water transfers from the unfrozen zone to the frozen zone. Meanwhile, the diminishing water in the unfrozen zone also led to the formation of negative pore water pressure, and liquid water was absorbed from the external water source. A frozen

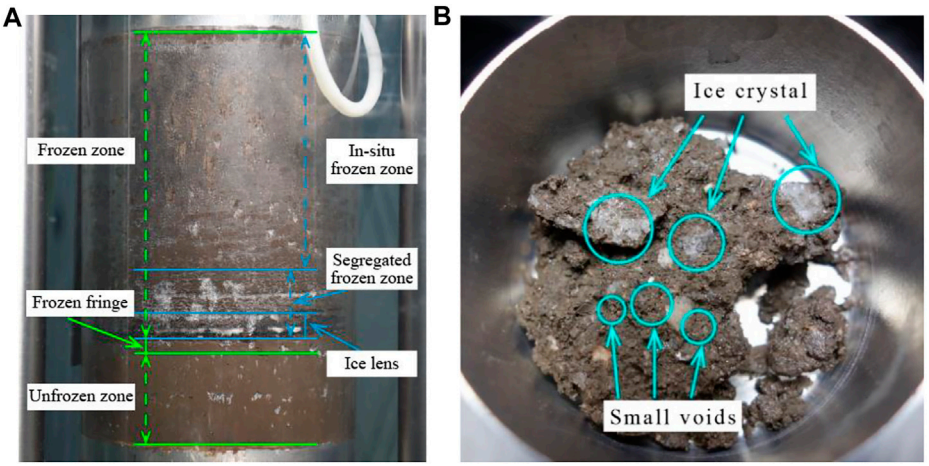

FIGURE 8 | Phase change of migrated water. **(A)** Ice lens formation in the clay; **(B)** large pore ice crystal and small empty voids in the CGS.

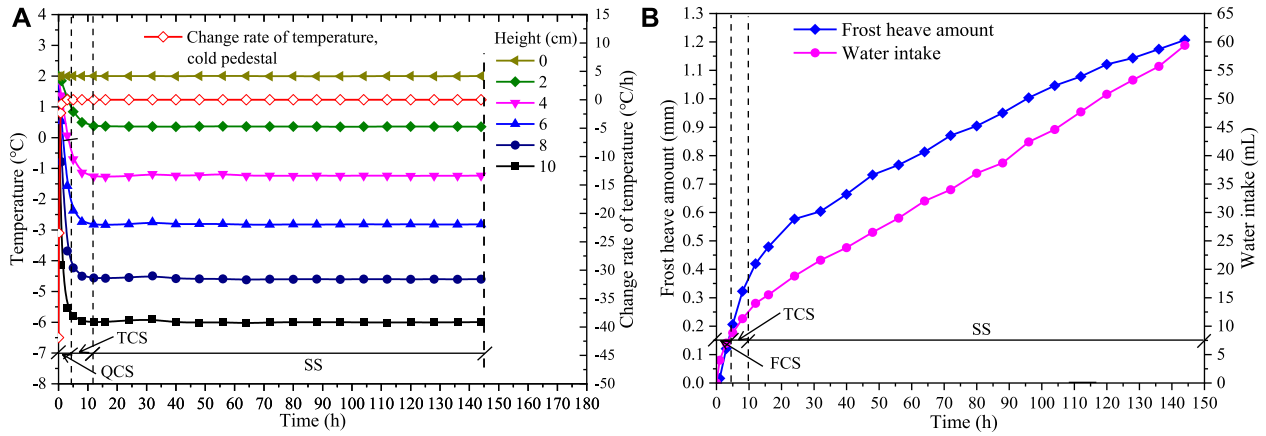

FIGURE 9 | Freezing results of CGS sample. **(A)** Variations of soil temperature and change rate of temperature; **(B)** variations of frost heave and water intake.

fringe of transition existed between the frozen zone and the unfrozen zone, where the phase change of pore water occurred. The frozen fringe temporarily stored the water transferred from the unfrozen zone and provided the water source for upward water migration. The void of clay was small, and easy to fill with pore ice. When the pore pressure exceeded the sum of the overburden pressure and separation pressure, the pore ices were integrated into a whole and formed an ice lens (Nixon, 1991; Thomas et al., 2009). Because of the blocking effect of the ice lens on unfrozen water migration, water that migrated from the unfrozen zone accumulated at the bottom of the ice lens. As a result, the water absorbed from the outside water source further changed into an ice lens, and the frost heave amount progressively increased with the growth of the ice lens. **Figure 8A** shows the typical ice lens formation of freezing clay at 96 h.

Frost Heave Characteristics of Coarse-Grained Soil

The experimental results for the CGS sample are shown in **Figure 9**. Similar to the freezing clay sample, the cooling process of the CGS sample can also be divided into three stages: the QCS, TCS, and SS (**Figure 9A**). The soil bottom temperature was maintained at +2°C, and the soil temperature at other heights decreased as the soil top temperature decreased. The closer to the top, the larger the cooling rate. Increases in the frost heave and water intake rates were observed immediately during freezing. In the SS, the soil temperature of the frozen zone at different heights fluctuated slightly and then remained stable. The frozen depth, frost heave rate, and water intake rate also gradually tended to become stable. The final frozen depth and heave amount were 75.5 and 1.2 mm, respectively. The final water intake and the frost heave ratio were 59.4 ml and 1.60%, respectively.

The states of the CGS column during freezing are shown in **Figure 10**. At the start of freezing, a small amount of water drop was found on the inner surface of the sample cell, which was produced by vapor condensation during the constant-temperature stage. The unfrozen and frozen zones showed no

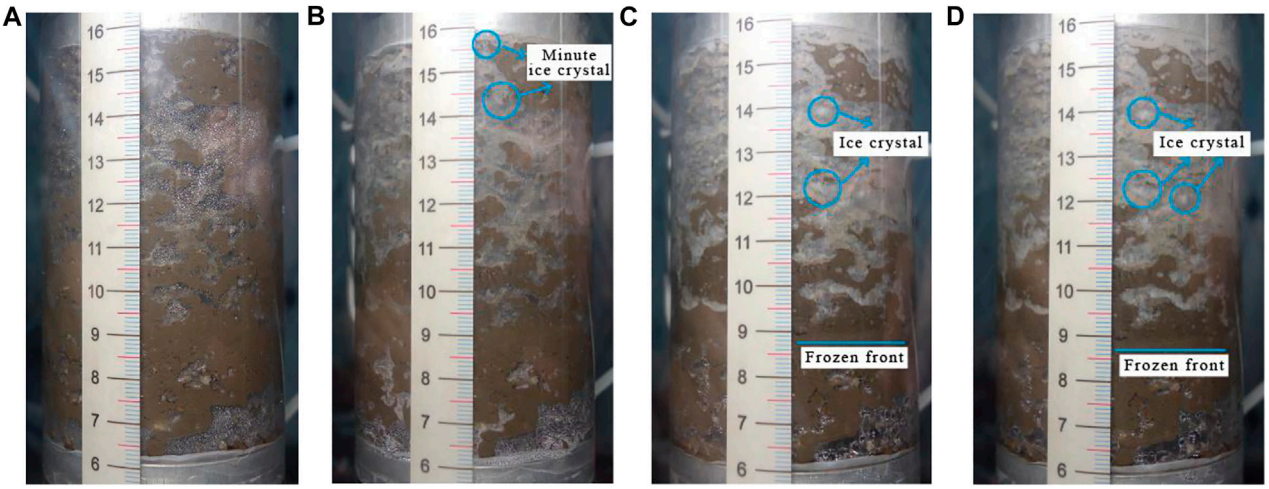

FIGURE 10 | States of CGS sample at **(A)** 0 h; **(B)** 10 h; **(C)** 96 h; and **(D)** 144 h.

distinct difference at 10 h because of the short freezing duration (**Figure 10B**). The liquid water migrated to the frozen zone under temperature gradients, leading to the formation of minute pore ice crystals between the soil particles in the frozen zone. At 96 and 144 h, the ice crystal size further increased with the freezing of migrating liquid water (**Figures 10C,D**). The soil void was filled with ice crystals that changed from migrating water (**Figure 8B**). The pore ice bulk was much less than the CGS particle bulk, leading to the pore pressure being insufficient to resist the sum of the overburden pressure and separation pressure. Even though the large voids were filled with pore ices, partial small voids were still empty without any ice crystals and were interconnected (**Figure 8B**). Ultimately, no visible ice lenses were detected within the frozen fringe.

Comparing the frost heave characteristic diversities between the clay soil and the CGS, it was shown that the water absorbed from outside water source mainly changed into pore ice for CGS, while it mainly changed into an ice lens for clay soil. The pore ice in the CGS was dispersed and not integrated into a whole, which was detrimental to the formation of an ice lens. Thus, the frost heave amount of the CGS was much less than that of the clay soil.

Based on the thermal boundary condition of the CGS sample, it can be concluded the temperature distribution along the soil column depth was nearly linear in the SS. The temperature distribution of the clay sample was similar to that of the CGS sample. One can conclude that the final frozen depth of the clay soil column was approximately 75.0 mm, and the corresponding frozen heave ratio was 25.73%. Under the same temperature conditions, even when the water intake amounts were very close, the frost heave amount and frost heave ratio of the CGS were much lower than those of the natural clay soil. This experimental result shows that replacing natural soil with CGS is a possibility for railway construction. To optimize the anti-frost effect of CGS in HSR embankments, the influence of fines content, initial water content, and grain size distribution of coarse particles on the frost heave ability of the CGS were investigated, as discussed in *Variations in Frost Heave With Soil Composition*.

VARIATIONS IN FROST HEAVE WITH SOIL COMPOSITION

The test samples, apparatuses, and procedures were the same as those in the frost heave test of the CGS, as described in the *Test Description*. The test scheme is listed in **Table 1**. Samples S1–S5 were prepared to study the influence of fines content on the frost susceptibility of CSG, samples S6, S2, and S7 were prepared to study the influence of initial water content, and samples S5 and S8–S10 were prepared to study the influence of the grain size distribution of coarse particles. The mass percentages of the certain-size grains of samples S5 and S8–S10 are presented in **Table 2**. The grain size distributions of the coarse particles of samples S1–S7 are the same. The grain gradation of the other samples with different fines contents can also be determined by combining with the grain gradation of sample S5. Sample S7 is the CGS sample described in *Frost Heave Characteristics of Coarse-Grained Soil*. The uniformity coefficient and coefficient of curvature for samples S5 and S8–S10 are listed in **Table 2**.

Effects of Fines Content and Initial Water Content

The three distribution models of the CGS with a given fines content are presented in **Figure 11**. The CGS without fines grains (**Figure 11A**), owing to its large voids, has a weak water retention ability and low matrix suction; thus, water migration along the coarse grain surface is difficult. In this case, the frost heave deformation is small and mainly in the pattern of *in-situ* frost heave. For the CGS with partial fines (**Figure 11B**), the void size between coarse grains is reduced and the matrix suction increases correspondingly. The external water is absorbed into the frozen soil, leading to the formation of pore ice. When the pore ice size increases to a certain extent, it begins to push the soil aggregate and support the overburden, bringing macroscopic heave of the CGS. Moreover, the void size further decreases, while the matrix suction and water seepage capacity further increase with the

TABLE 1 | Frost heave test schemes for CGS fillings.

Sample	Grain size distribution of coarse particles	Initial water content (%)	Fines content (%)	Porosity (%)	Temperature boundary of soil sample		Well or poorly graded
					Top (°C)	Bottom (°C)	
S1	Size grade I	8	4.0	23.8	−6	2	Well
S2	Size grade I	8	5.9	24.0	−6	2	Well
S3	Size grade I	8	9.3	24.2	−6	2	Well
S4	Size grade I	8	11.9	24.4	−6	2	Well
S5	Size grade I	8	14.2	24.6	−6	2	Poorly
S6	Size grade I	6	5.9	24.0	−6	2	Well
S7	Size grade I	10	5.9	24.0	−6	2	Well
S8	Size grade II	8	14.2	24.6	−6	2	Well
S9	Size grade III	8	14.2	24.6	−6	2	Well
S10	Size grade IV	8	14.2	24.6	−6	2	Poorly

TABLE 2 | Mass percentage of the certain-size grains.

Sample	Grain size distribution of coarse particles	Grain size (mm)										Uniformity coefficient	Coefficient of curvature
		10	5	2	0.5	0.25	0.075	0.05	0.02	0.01	0		
S5	Size grade I	32	24	8	8	8	4.9	7.8	2.8	4.5	0.5	128.57	0.89
S8	Size grade II	40	24	16	4	4	4.9	7.8	2.8	4.5	0.25	178.57	2.57
S9	Size grade III	16	16	16	16	16	4.9	7.8	2.8	4.5	0.25	35.71	1.03
S10	Size grade IV	40	24	16	0	0	4.9	7.8	2.8	4.5	0.075	178.57	1.45

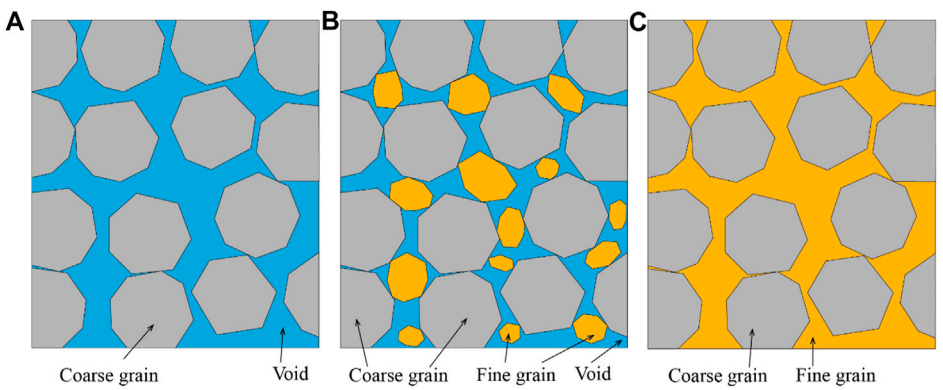

FIGURE 11 | Distribution models of CGS. **(A)** CGS without fines; **(B)** CGS without partial fines; and **(C)** CGS with saturated fines.

TABLE 3 | Frost heave test results for samples S1–S7 after freezing for 144 h.

Sample	Fines content (%)	Initial water content (%)	Frost depth (mm)	Frost heave amount (mm)	Frost heave ratio (%)	Water intake (ml)
S1	4.0	8.0	73.24	0.58	0.79	30.60
S2	5.9	8.0	76.21	0.84	1.10	31.00
S3	9.3	8.0	75.50	1.12	1.48	45.80
S4	11.9	8.0	76.74	1.36	1.77	51.00
S5	14.2	8.0	77.62	1.46	1.88	56.00
S6	5.9	6	77.30	0.68	0.88	40.2
S7	5.9	10	75.50	1.21	1.60	49.4

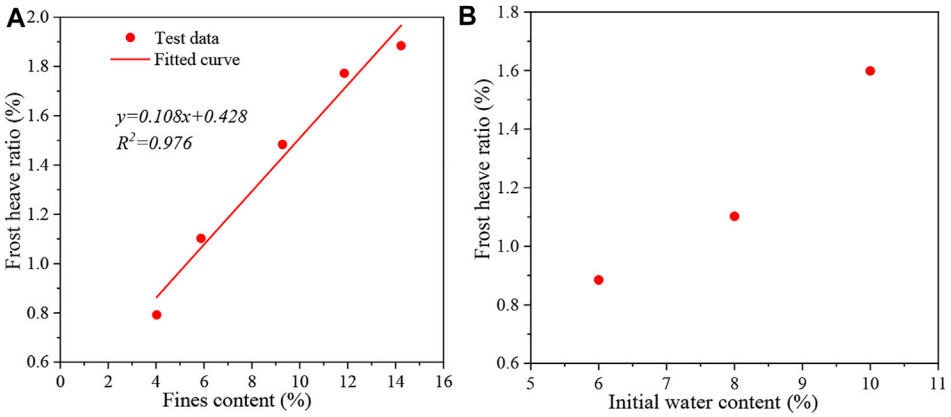

FIGURE 12 | The influence of fines content and initial water content. **(A)** Relationship of frost heave ratio and fines content; **(B)** relationship of frost heave ratio and initial water content.

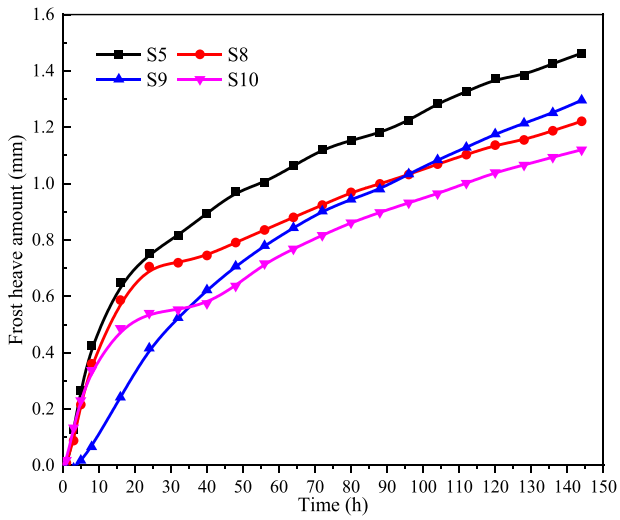

FIGURE 13 | Frost heave for samples with various grain size distributions of coarse particles.

increase in fines content, causing an increase in the water intake amount and pore ice content (**Table 3**). Based on the three models, the experimental results are shown in **Figure 12A**. The frost heave ratio of the CGS in the experiments increased nearly linearly with the increase in fines content. According to the fitting function, the frost heave ratio of the CSG was less than 1% when the fines content was less than 5.3%. At this point, the CSG could be considered a non-frost-susceptible filling. In the case of CGS with saturated fines (**Figure 11C**), where coarse grains were floating in the fine grain, significant frost heave occurred. When the fines content was far more than the coarse grain content, an ice lens formed in the water-saturated freezing CGS (Li et al., 2017).

One can conclude that the fines content strongly affected the water migration, pore ice formation, and frost heave ratio of the CGS, i.e., the fines content improved the frost susceptibility of the CGS, even when it was water unsaturated.

According to the test results of samples S6, S2, and S7, the frost heave ratio increased with initial water content, as shown in **Figure 12B**. The hydraulic conductivity of the unsaturated CGS is (Babu and Srivastava, 2007):

$$K = CD^2 \frac{\gamma_w}{\eta} \frac{e^3}{1+e} \tag{2}$$

$$e = \frac{G_s(1+w)}{\rho} - 1 \tag{3}$$

where K is the hydraulic conductivity of CGS; C is a constant that depends on the compaction method; D is the effective particle size and can be taken as d_{10}; γ_w and η are the unit weight and viscosity coefficient of water, respectively; e is the void ratio; G_s is the specific gravity of soil grains; ρ is the soil density; and w is the water content of soil.

According to **Eq. 2** and **Eq. 3** the hydraulic conductivity of the CGS increases with an increase in water content. As a result, the rate of water migration increases, causing the formation rate of pore ice and the frost heaving rate to increase. Therefore, the total heave amount is expected to increase with increasing water content, as shown in **Table 3**. Meanwhile, the increasing rate of water migration brings more latent heat of the phase change that occurs in the frozen fringe. The increased water content indicates a greater release of latent heat, which inhibits the advancement of the frost front. Therefore, the frozen depth of the CGS is expected to decrease as the water content increases (**Table 3**).

Effect of Grain Size Distribution of Coarse Particles

Figure 13 shows the variations in the frost heave amount for four samples with different grain size distributions of coarse particles during the freezing process. Under the same controlling conditions, the frost heave rate of sample S9 was lower than

TABLE 4 | Test results for samples S5 and S8–S10 after freezing for 144 h.

Sample	Grain size distribution of coarse particles	Frost depth (mm)	Frost heave (mm)	Frost heave ratio (%)
S5	Size grade I	77.62	1.46	1.88
S8	Size grade II	77.95	1.22	1.57
S9	Size grade III	78.13	1.30	1.66
S10	Size grade IV	77.60	1.13	1.45

that of the other samples in the early freezing stage. This was mainly because sample S9 had the highest sand content, especially the medium sand and fine sand. The bound water content was the highest, while the free water content was the lowest. Frost heave mainly occurred in the pattern of *in-situ* frost heave during the early stage. In contrast, the heave rates of samples S5 and S9 were higher than those of samples S8 and S10 in the stable stage. This can be attributed to the lower uniformity coefficient and less difference between neighboring granule group contents in samples S5 and S9 (**Table 2**). The matrix suction increased with the decrease in voids size. As a result, for the porous samples S5 and S9, the water was mainly migrated in the liquid pattern at the stable stage, and the frost heave amounts were larger than those of samples S8 and S10.

The medium sand content and fine sand content of sample S10 were 8% less than those of sample S5. In agreement with this, the frost heave ratio of sample S10 was 0.43% less than that of sample S5 (**Table 4**). It follows that the sand content was another limiting factor for the frost susceptibility of CGS, in addition to the fines content.

DISCUSSION OF EMBANKMENT FROST HEAVE PREVENTION

As discussed in *Test Results and Analysis*, the frost heave ratio of the natural flat ground was much lower than that of the experimental freezing clay. This was because the compacted clay soil in the indoor test had fewer voids and a relatively higher thermal conductivity, which was beneficial for moving the freezing front. Furthermore, the distance between the frozen soil and water supply system in the indoor test was much less than that in the natural ground, meaning that the external water was more easily to be absorbed into the frozen zone and changed into ice. Nevertheless, the frost heave ratio difference between field monitoring and indoor tests did not affect the tests to measure the frost heave ability of the foundation soil and CGS filling.

According to the field monitoring data, under the same temperature and soil type conditions, the groundwater supply was observed to be the primary factor for the frost heave difference between flat ground and hillslope sections. In addition, the infiltration of rainfall is another water supply way water can be supplied for soil segregation frost heaving. When rainfall and snowmelt water accumulate in the embankment fill, even the well-graded A/B group layer can cause obvious frost heaving at negative temperatures. This was verified by the frost heave test. Under suitable water conditions, sample S5 produced a significant frost heave ratio of 1.88%, which was larger than the non-frost-susceptible criterion of 1% (Konrad and Lemieux, 2005). One possible reason for the water accumulation is that water flows from the top surface into the filling layer when the sealing of the track plate fails. Second, the highly compacted CGS filling layer with high fines and sand content has a strong water retention ability and relatively low water seepage capacity. This layer provides a perfect location for water accumulation. Third, the commonly used compound geomembrane in the HSR embankment, which is used to prevent infiltration of groundwater, blocks the rainwater seepage path. As a result, water accumulation may occur above the upper surface of the geomembrane (Miao et al., 2020). Accordingly, two methods have been suggested to disrupt local water accumulation. One is to strictly close the surface and the side of the embankment to prevent external water from seeping into the embankment. The other is to install embankment subdrainage holes to drain the accumulated water from the filling layers.

In the application of the soil-replacement method, fines content and water content are considered the two main influential factors for the frost susceptibility of the CGS. Konrad and Lemieux (2005), Akagawa et al. (2017), and Gao et al. (2018) reported that the frost heave susceptibility of the CGS increased with an increase in fines content and water content. This finding was also confirmed in the above test. The results suggest that CGS filling should strictly control fines content and water content. When the grain size distributions were different, the frost heave amount and frost heave ratio of sample S5 were the largest, while those of sample S10 were the lowest (**Table 4**). The frost heave mitigation effect of the poorly graded CGS was better than that of the well-graded CGS under the same conditions.

However, when the freezing front passes through the CGS filling and infiltrates the frost-susceptible clay, embankment frost heave still can occur in the case of shallow groundwater. Furthermore, rain-induced groundwater level rise further shortens the water migration distance if precipitation is enhanced. Therefore, to reduce the water migration capacity, the depth of soil replacement should not only exceed the maximum frost depth of the CGS filling layer but also include partial natural clay beyond the frost depth.

In short, the frost heave control of the HSR embankment should have three parts: 1) replacing natural clay with weakly frost-susceptible CGS filling; 2) eliminating the local water accumulation in the filling layer; and 3) reducing the water migration capacity of soil between the freezing layer and groundwater as much as possible.

CONCLUSION

In this study, the variations in ground temperature, deformation, soil moisture, and groundwater table were monitored to analyze the frost heave characteristics of the embankment foundation soil in the Zoige Wetland section of the Xining–Chengdu HSR line. Based on these observations and local geological environment data, a subgrade soil-replacement method was proposed to mitigate the frost heave deformation of railway embankments. Two contrasting frost heave tests were conducted on clay soil and CGS to prove the feasibility and validity of this method. Further experiments were performed to optimize the anti-frost effects of the replacement method. The conclusions can be drawn as follows:

- For natural flat ground and hillslope in the Zoige Wetland, the maximum frost heave ratios reached 6.10 and 1.45%, respectively. The groundwater supply condition was the primary factor for the different frost heave at these two sites.
- Under the same conditions, even when the water intake amount was very close, the frost heave ratio of the CGS was far less than that of natural, clay-rich soil. Combined with the local geological environment and engineering construction conditions, the soil-replacement method was proven to be effective in mitigating the frost heave deformation of embankment filling.
- The frost susceptibility of the CGS was proportional to the fines content and initial water content. The frost heave mitigation effect of the poorly graded CGS was better than that of the well-graded CGS under the same conditions. It is suggested that the replacement method should strictly control the fine content and water content, and preferentially use poorly graded CGS filling.
- The replacement of the CGS filling layer should also incorporate other measures to disrupt local rainwater accumulation and reduce the water migration capacity of soil between the freezing filling layer and groundwater.

DATA AVAILABILITY STATEMENT

The original contributions presented in the study are included in the article/**supplementary material**, further inquiries can be directed to the corresponding authors.

AUTHOR CONTRIBUTIONS

FN: Conceptualization, Methodology, Validation, Data curation, Formal analysis, Writing - original draft. HH: Conceptualization, Methodology, Validation, Writing - review & editing. ML: Writing - review & editing. QM: Writing - review & editing. WS: Writing - review & editing.

FUNDING

This research was supported by the Strategic Priority Research Program of the Chinese Academy of Sciences (Grant No. XDA19070504), Science and Technology Service Network Initiative of CAS (No. KFJ-STS-ZDTP-037), National Natural Science Foundation of China (41901074).

SUPPLEMENTARY MATERIAL

The Supplementary Material for this article can be found online at: https://www.frontiersin.org/articles/10.3389/feart.2021.678655/full#supplementary-material

REFERENCES

Akagawa, S., Hori, M., and Sugawara, J. (2017). Frost Heaving in Ballast Railway Tracks. *Proced. Eng.* 189, 547–553. doi:10.1016/j.proeng.2017.05.087

Babu, G. L. S., and Srivastava, A. (2007). A Procedure for the Design of Protective Filters. *Can. Geotech. J.* 44 (4), 490–495. doi:10.1139/t07-005

Everett, D. H. (1961). The Thermodynamics of Frost Damage to Porous Solids. *Trans. Faraday Soc.* 57, 1541–1551. doi:10.1039/tf9615701541

Gao, J., Lai, Y., Zhang, M., and Feng, Z. (2018). Experimental Study on the Water-Heat-Vapor Behavior in a Freezing Coarse-Grained Soil. *Appl. Therm. Eng.* 128, 956–965. doi:10.1016/j.applthermaleng.2017.09.080

Gilpin, R. R. (1980). A Model for the Prediction of Ice Lensing and Frost Heave in Soils. *Water Resour. Res.* 16 (5), 918–930. doi:10.1029/wr016i005p00918

Harlan, R. L. (1973). Analysis of Coupled Heat-Fluid Transport in Partially Frozen Soil. *Water Resour. Res.* 9 (5), 1314–1323. doi:10.1029/wr009i005p01314

Jin, H. W., Lee, J., Ryu, B. H., Shin, Y., and Jang, Y. E. (2019). Experimental Assessment of the Effect of Frozen Fringe Thickness on Frost Heave. *Geomech Eng.* 19 (2), 193–199. doi:10.12989/gae.2019.19.2.193

Jin, Y. (2007). Theory and Application for Retrieval and Fusion of Spatial and Temporal Quantitative Information from Complex Natural Environment. *Front. Earth Sci. China* 1 (3), 284–298. doi:10.1007/s11707-007-0035-0

Konrad, J.-M. (2008). Freezing-induced Water Migration in Compacted Base-Course Materials. *Can. Geotech. J.* 45, 895–909. doi:10.1139/t08-024

Konrad, J.-M., and Lemieux, N. (2005). Influence of Fines on Frost Heave Characteristics of a Well-Graded Base-Course Material. *Can. Geotech. J.* 42 (2), 515–527. doi:10.1139/t04-115

Konrad, J.-M., and Morgenstern, N. R. (1982). Prediction of Frost Heave in the Laboratory during Transient Freezing. *Can. Geotech. J.* 19 (3), 250–259. doi:10.1139/t82-032

Konrad, J.-M., and Morgenstern, N. R. (1981). The Segregation Potential of a Freezing Soil. *Can. Geotech. J.* 18 (4), 482–491. doi:10.1139/t81-059

Li, A., Niu, F., Zheng, H., Akagawa, S., Lin, Z., and Luo, J. (2017). Experimental Measurement and Numerical Simulation of Frost Heave in Saturated Coarse-Grained Soil. *Cold Regions Sci. Techn.* 137, 68–74. doi:10.1016/j.coldregions.2017.02.008

Li, X., Cheng, G., Jin, H., Kang, E., Che, T., Jin, R., et al. (2008). Cryospheric Change in China. *Glob. Planet. Change* 62 (3), 210–218. doi:10.1016/j.gloplacha.2008.02.001

Lin, Z., Niu, F., Li, X., Li, A., Liu, M., Luo, J., et al. (2018). Characteristics and Controlling Factors of Frost Heave in High-Speed Railway Subgrade, Northwest China. *Cold Regions Sci. Techn.* 153, 33–44. doi:10.1016/j.coldregions.2018.05.001

Liu, H., Niu, F., Niu, Y., Xu, J., and Wang, T. (2016). Effect of Structures and Sunny-Shady Slopes on thermal Characteristics of Subgrade along the Harbin-Dalian Passenger Dedicated Line in Northeast China. *Cold Regions Sci. Techn.* 123, 14–21. doi:10.1016/j.coldregions.2015.11.007

Mao, X., Miller, C., Hou, Z., and Khandker, A. (2014). Experimental Study of Soil Water Migration in Freezing Process. *Geotech Test. J.* 37 (3), 436–446. doi:10.1520/gtj20130119

Miao, Q., Niu, F., Lin, Z., Luo, J., and Liu, M. (2020). Comparing Frost Heave Characteristics in Cut and Embankment Sections along a High-Speed Railway in Seasonally Frozen Ground of Northeast China. *Cold Regions Sci. Techn.* 170, 102921. doi:10.1016/j.coldregions.2019.102921

Miller, R. D. (1972). Freezing and Heaving of Saturated and Unsaturated Soils. *Highw. Res. Rec.* 393, 1–11.

Niu, F., Li, A., Luo, J., Lin, Z., Yin, G., Liu, M., et al. (2017). Soil Moisture, Ground Temperatures, and Deformation of a High-Speed Railway Embankment in Northeast China. *Cold Regions Sci. Techn.* 133, 7–14. doi:10.1016/j.coldregions.2016.10.007

Nixon, J. F. (1991). Discrete Ice Lens Theory for Frost Heave in Soils. *Can. Geotech. J.* 28 (6), 843–859. doi:10.1139/t91-102

O'Neill, K., and Miller, R. D. (1985). Exploration of a Rigid Ice Model of Frost Heave. *Water Resour. Res.* 21 (3), 281–296.

Peppin, S. S. L., and Style, R. W. (2012). The Physics of Frost Heave and Ice-Lens Growth. *Vadose Zone J.* 12 (1), 1–12. doi:10.2136/vzj2012.0049

Sheng, D., Axelsson, K., and Knutsson, S. (1995). Frost Heave Due to Ice Lens Formation in Freezing Soils. *Nordic Hydrol.* 26 (2), 125–146. doi:10.2166/nh.1995.0008

Sheng, D., Zhang, S., Niu, F., and Cheng, G. (2014). A Potential New Frost Heave Mechanism in High-Speed Railway Embankments. *Géotechnique* 64 (2), 144–154. doi:10.1680/geot.13.p.042

Sheng, D., Zhang, S., Yu, Z., and Zhang, J. (2013). Assessing Frost Susceptibility of Soils Using PCHeave. *Cold Regions Sci. Techn.* 95, 27–38. doi:10.1016/j.coldregions.2013.08.003

Song, L., Li, H., Wang, K., Wu, D., and Wu, H. (2014). Ecology of Testate Amoebae and Their Potential Use as Palaeohydrologic Indicators from Peatland in Sanjiang Plain, Northeast China. *Front. Earth Sci.* 8 (4), 564–572. doi:10.1007/s11707-014-0435-x

Taber, S. (1929). Frost Heaving. *J. Geol.* 37 (5), 428–461. doi:10.1086/623637

The National Standards Compilation Group of the People's Republic of China (2014). *GB 50324—2014 Code for Engineering Geological Investigation of Frozen Ground*. Beijing, China: China Planning Press. (in Chinese).

The National Standards Compilation Group of the People's Republic of China (2011). *JGJ 118—2011 Code for Design of Soil and Foundation of Building in Frozen Soil Region*. Beijing, China: China Architecture Publishing. (in Chinese).

Thomas, H. R., Cleall, P., Li, Y.-C., Harris, C., and Kern-Luetschg, M. (2009). Modelling of Cryogenic Processes in Permafrost and Seasonally Frozen Soils. *Géotechnique* 59 (3), 173–184. doi:10.1680/geot.2009.59.3.173

Wang, Q., Liu, J., Zhu, X., Liu, J., and Liu, Z. (2016). The experiment Study of Frost Heave Characteristics and gray Correlation Analysis of Graded Crushed Rock. *Cold Regions Sci. Techn.* 126, 44–50. doi:10.1016/j.coldregions.2016.03.003

Wang, T., Zhou, G., Wang, J., and Wang, D. (2020). Impact of Spatial Variability of Geotechnical Properties on Uncertain Settlement of Frozen Soil Foundation Around an Oil Pipeline. *Geomech Eng.* 20 (1), 19–28. doi:10.12989/gae.2020.20.1.019

Wu, X. Y., Niu, F. J., Lin, Z. J., Luo, J., Zheng, H., and Shao, Z. J. (2018). Delamination Frost Heave in Embankment of High Speed Railway in High Altitude and Seasonal Frozen Region. *Cold Regions Sci. Techn.* 153, 25–32. doi:10.1016/j.coldregions.2018.04.017

Xu, X., Bai, R., Lai, Y., Zhang, M., and Ren, J. (2020). Work Conjugate Stress and Strain Variables for Unsaturated Frozen Soils. *J. Hydrol.* 582, 124537. doi:10.1016/j.jhydrol.2019.124537

Yue, Z., Ge, J., Li, Z., and Liu, Y. (2007). Study on Settlement of Unprotected Railway Embankment in Permafrost. *Cold Regions Sci. Techn.* 48 (1), 24–33. doi:10.1016/j.coldregions.2006.09.003

Zhang, S., Sheng, D., Zhao, G., Niu, F., and He, Z. (2016). Analysis of Frost Heave Mechanisms in a High-Speed Railway Embankment. *Can. Geotech. J.* 53 (3), 520–529. doi:10.1139/cgj-2014-0456

Zuo, D., Luo, P., Yang, H., Mou, C., Li, Y., Mo, L., et al. (2019). Assessing the Space Neighborhood Effects and the protection Effectiveness of a Protected Area - a Case Study from Zoige Wetland National Nature Reserve. *Chin. J. Appl. Environ. Biol.* 25 (4), 0854–0861. (in Chinese).

Conflict of Interest: The authors declare that the research was conducted in the absence of any commercial or financial relationships that could be construed as a potential conflict of interest.

The reviewer QW declared a shared affiliation with one of the authors, ML, to the handling editor at time of review.